Journal of Inflammation Research

Dovepress
Taylor & Francis Group

Open Access Full Text Article

ORIGINAL RESEARCH

# Apigenin Suppresses NLRP3 Inflammasome Activation and Pyroptosis and Promotes Functional Recovery by Promoting Mitophagy in Experimental Spinal Cord Injured Rats

Zuomeng Wu[1,2,*], Yunxiao Fang[1,2,*], Yixiang Dong[1,2], Yue Qin[1,2], Ao Liu[1,2], Tianyu Han[1,2], Peiwen Song[1,2], Cailiang Shen[1–3]

[1]Department of Orthopedics (Spinal Surgery), The First Affiliated Hospital of Anhui Medical University, Hefei, 230032, People's Republic of China; [2]Laboratory of Spinal and Spinal Cord Injury Regeneration and Repair, The First Affiliated Hospital of Anhui Medical University, Hefei, 230032, People's Republic of China; [3]Anhui Province Research Center for the Clinical Application of Digital Medical Technology, The First Affiliated Hospital of Anhui Medical University, Hefei, Anhui, 230022, People's Republic of China

*These authors contributed equally to this work

Correspondence: Cailiang Shen, Email shencailiang@ahmu.edu.cn



**Background:** Secondary damage following spinal cord injury (SCI) is closely associated with pyroptosis and mitochondrial dysfunction. Apigenin (API), a natural flavonoid, possesses notable anti-inflammatory and antioxidant properties. However, whether API can inhibit microglial pyroptosis via the mitophagy pathway, thereby exerting neuroprotective effects, remains unclear. This study aimed to elucidate the mechanism by which API mitigates post-SCI inflammatory responses through modulation of the mitophagy-NLRP3 axis.

**Methods:** Neurological recovery was assessed using the Basso, Beattie, and Bresnahan scale, neuroelectrophysiological recordings, and histological analyses. The effects of API on NLRP3 inflammasome activation, reactive oxygen species (ROS) generation, and mitochondrial membrane potential were assessed using ELISA, quantitative PCR, immunofluorescence, and JC-1 staining.

**Results:** API significantly improved locomotor function in SCI rats, reduced scar formation, and promoted axonal regeneration. Mechanistically, API downregulated NLRP3/ gasdermin D expression in microglia, reduced the release of inflammatory factors, and enhanced mitophagy. Notably, the protective effects of API were reversed by Mdivi-1 and mimicked by Urolithin A, confirming that mitophagy is the primary mechanism mediating API's anti-pyroptotic effects.

**Conclusion:** API attenuates microglial pyroptosis and facilitates SCI repair by enhancing mitophagy-mediated clearance of damaged mitochondria and suppressing activation of the ROS/NLRP3 inflammasome pathway in rats. These findings provide important preclinical evidence supporting the development of multi-target neuroprotective strategies derived from natural compounds.

**Plain Language Summary:**

- API effectively suppresses NLRP3 inflammasome activation and mitigates microglial pyroptosis.
- API enhances mitophagy in microglia following SCI.
- API inhibits pyroptosis through mitophagy-mediated regulation of NLRP3 activation.
- API significantly promotes locomotor recovery and neural regeneration in spinal cord-injured rats.

**Keywords:** spinal cord injury, apigenin, mitophagy, pyroptosis

## Introduction

Spinal cord injury (SCI) is among the most severe consequences of spinal trauma, arising from either traumatic events or non-traumatic causes. SCI results in both structural and functional disruption of the spinal cord, leading to motor, sensory, and

Received: 24 June 2025
Accepted: 26 September 2025
Published: 8 October 2025

**Graphical Abstract**

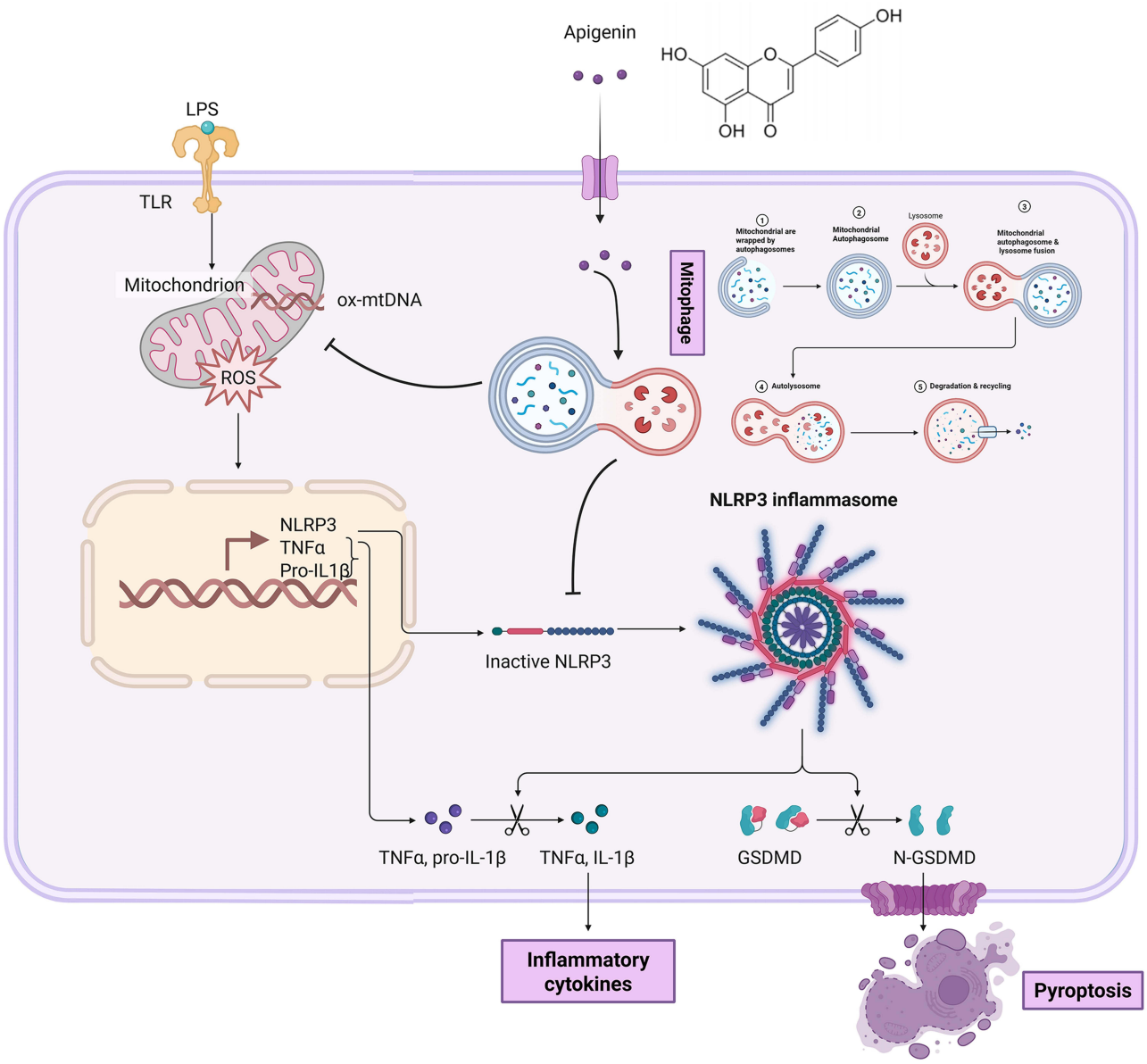


autonomic impairments below the level of injury.[1,2] It was reported that there are currently 759,302 patients living with traumatic SCI in China, with approximately 66,374 new cases occurring annually.[3] In the United States, around 17,000 new SCI cases are reported each year. The medical costs during the first year alone for a patient with high-level tetraplegia can exceed one million US dollars.[4] Severe SCI places considerable physical and psychological burdens on affected individuals, as well as imposing significant economic challenges on their families. Current standard management in the acute phase includes surgical decompression with spinal stabilization, followed by sustained rehabilitation interventions.[5] However, these strategies primarily focus on reducing secondary injury, maintaining spinal integrity and stability, and supporting compensatory functional adaptation—rather than promoting neural regeneration or repairing disrupted neural circuits. Although existing treatments are administered promptly after injury, they remain limited in their ability to restore neurological function.

Pathologically, SCI is classified into primary injury—direct mechanical damage—and secondary injury, which involves a cascade of inflammatory and oxidative stress responses occurring from hours to weeks post-injury.[6,7] Following the primary insult, local ischemia and hypoxia induce mitochondrial dysfunction, leading to an accumulation of reactive oxygen species (ROS) and leakage of mitochondrial DNA (mtDNA), which subsequently activate pattern recognition receptors within the innate immune system.[8–10] Microglia and infiltrating macrophages rapidly polarise towards a pro-inflammatory (M1) phenotype, exacerbating blood-spinal cord barrier disruption and neuronal apoptosis through the release of inflammatory cytokines such as interleukin-1β (IL-1β) and IL-18.[11,12]

Maintaining a dynamic balance in mitochondrial quality control is essential for inflammation regulation. Mitophagy is a critical quality control mechanism for selectively removing damaged mitochondria. Dysfunctional mitochondria are identified via the PINK1/Parkin pathway or receptor-mediated routes (eg, BNIP3 and FUNDC1) and subsequently degraded via autophagosome fusion.[13–16] Recent studies indicate that defective mitophagy promotes the cytoplasmic accumulation of mtDNA and ROS, which directly activates the NLRP3 inflammasome.[17,18] In neurodegenerative disease models, inhibiting microglial glutamine metabolism enhances mitophagy, thereby reducing ROS levels and suppressing NLRP3 inflammasome activation.[19–21] Conversely, excessive mitophagy may deplete cellular energy reserves, worsening cell death.[22,23] However, the spatiotemporal dynamics of mitophagy in SCI and its interplay with the NLRP3 inflammasome remain poorly understood.

A central event in pyroptosis is activation of the NOD-like receptor pyrin domain-containing 3 (NLRP3) inflammasome. Pyroptosis is a form of programmed cell death characterised by membrane pore formation, cellular swelling and lysis, and the release of pro-inflammatory cytokines.[24,25] It functions as a key immune defence mechanism against tissue injury and is implicated in various inflammation-related disorders.[26–28] Damage-associated molecular patterns (DAMPs), such as ATP and mtDNA, stimulate the expression of NLRP3, apoptosis-associated speck-like protein (ASC), and caspase-1 via Toll-like receptors and the nuclear factor-κB (NF-κB) signalling pathway.[24,29,30] Subsequent ROS accumulation or ion channel dysregulation triggers NLRP3 inflammasome activation. Active caspase-1 cleaves gasdermin D (GSDMD), which forms membrane pores that mediate pyroptotic cell death and inflammatory mediator release.[31–33] Notably, inhibiting the NLRP3/caspase-1 axis has been shown to significantly attenuate inflammation and neuronal loss in SCI models.[34,35]

Identifying effective strategies to modulate the inflammatory microenvironment post-SCI is vital for promoting neural regeneration and functional recovery. Natural plant-derived compounds, valued for their bioactivity and low intrinsic toxicity, have gained attention in the treatment of inflammatory conditions. Apigenin (API), a widely studied natural flavonoid extracted from parsley, garlic, and chamomile, possesses potent anti-inflammatory, antioxidant, and antifibrotic properties.[36] Both in vitro and in vivo studies have demonstrated that API effectively alleviates doxorubicin-induced myocardial pyroptosis and cardiotoxicity through direct targeting of GSK-3β and modulation of pyroptosis-related factor expression.[37] Furthermore, API mitigates palmitic acid-induced pyroptosis in primary mouse hepatocytes by activating autophagy to remove damaged mitochondria.[38] Additionally, API exhibits protective effects against cisplatin-induced ototoxicity by reducing reactive oxygen species (ROS) accumulation and modulating apoptosis-related signaling pathways, including p53 and FoxO.[39] Evidence suggests that API alleviates lipotoxicity-induced NLRP3 inflammasome activation in macrophages by suppressing endoplasmic reticulum stress and restoring autophagic function.[40] Although Jin et al demonstrated that API inhibits fibrotic scar formation via the TGFβ/SMADs pathway in acute SCI,[41] its role in modulating microglial pyroptosis after SCI remains unclear. Furthermore, it is not yet known whether API influences NLRP3 inflammasome activity through mitophagy.

Accordingly, this study aimed to elucidate the molecular mechanisms by which API regulates the NLRP3 inflammasome and pyroptosis via mitophagy in both in vitro and in vivo models, thereby contributing to the development of multi-target neurorestorative therapies derived from natural compounds.

# Methods

## Animals and the SCI Model

Sprague-Dawley (SD) rats were obtained from the Animal Centre of Anhui Medical University (Hefei, China). Female SD rats aged 8–10 weeks and weighing approximately 220 g were selected to establish the traumatic spinal cord injury model. The model was generated following a previously published protocol from our group.[42] Briefly, animals were

randomly assigned to experimental groups, anesthetised with sodium pentobarbital (35 mg/kg), and the T9–T10 spinal cord segments were exposed. A complete bilateral compression injury was induced by applying Dumont forceps (tip width: 0.5 mm) for 5 s.[43,44] Successful model establishment following clamping is indicated by the presence of congestion and compression marks at the T10 level of the spinal cord, along with bilateral hindlimb twitching and tail elevation observed during the procedure (Figure 1A). Postoperative care included twice-daily antibiotic treatment and manual bladder expression. In the Sham group, only laminectomy was performed without spinal cord compression. API (MCE, HY-N1201, USA) was dissolved in 10% dimethyl sulfoxide (DMSO) (BS087, Biosharp, China), and SCI rats were intraperitoneally injected with API at 10 mg/kg/day or 50 mg/kg/day for 1 week post-surgery (referred to as API 10 and API 50 groups, respectively). All rats were maintained under specific pathogen-free conditions at the Animal Experiment Centre of Anhui Medical University (Hefei, China), with controlled temperature (22–24 °C), humidity (40–60%), and a 12-hour light/dark cycle. Food and water were provided ad libitum. All procedures were approved by the Animal Care and Use Committee of Anhui Medical University (LLSC 20242471).All animal experiments comply with the National Standards for Laboratory Animal Welfare issued by the Chinese government (GB/T 35892–2018) and the Guide for the Care and Use of Laboratory Animals (National Research Council, 8th Edition, 2011).All procedures comply with the ARRIVE guidelines.

## Basso, Beattie, and Bresnahan Score

The Basso, Beattie, and Bresnahan (BBB) open-field test was employed to evaluate hindlimb motor function in SCI rats. Two independent observers, blinded to group allocation, assessed locomotor recovery at days 1, 3, 7, 14, 21, and 28 post-injury.

## Neuroelectrophysiological Examination

Electrophysiological assessments were conducted 4 weeks after SCI. To record motor-evoked potentials (MEPs), a stimulating electrode was placed on the scalp, 2.5 mm anterior to the upper eyelid and 2.5 mm lateral to the midline, with a depth of 1 mm. The recording electrode was inserted into the gastrocnemius muscle, while the ground electrode was affixed to the skin of the back. All electrodes were connected to a bio-information acquisition system for data collection.

## Immunofluorescence Staining

For tissue processing, rats were perfused transcardially with cold phosphate-buffered saline (PBS), followed by 4% paraformaldehyde (PFA). Spinal cords were harvested, fixed in 4% PFA at 4°C for 24 h, and sectioned longitudinally into 4 μm-thick sections using a Leica RM2135 microtome (Leica, Germany), centred on the injury site. For tissue immunofluorescence, sections were blocked with 10% bovine serum albumin (BSA), incubated with primary antibodies overnight at 4°C, and subsequently with secondary antibodies for 1 h at room temperature. Following three PBS washes, nuclei were counterstained with 4',6-diamidino-2-phenylindole (DAPI), and images were captured using fluorescence microscopes (AxioVert A1 and Imager A2, Zeiss, Germany). For cell immunofluorescence, cells were fixed in 4% PFA for 30 min, permeabilised with 0.05% Triton X-100, blocked with 10% BSA, incubated with primary antibodies overnight at 4°C, and processed similarly.

The primary antibodies used were as follows: rabbit anti-NF for neurofilament (1:200; Abcam, United Kingdom), rabbit anti-Neun for neuron (1:200; Abcam, United Kingdom), rabbit anti-GFAP for astroglia (1:1000; Abcam, United Kingdom), mouse anti-IBA1 for microglia (1:200; Abcam, United Kingdom), rabbit anti-GSDMD (1:200; Abcam, United Kingdom), rabbit anti-LC3B (1:200; Abcam, United Kingdom), rabbit anti-P62 (1:200; Abcam, United Kingdom), and rabbit anti-NLRP3 (1:200; Abcam, United Kingdom). Alexa Fluor 488 (green, 1:100; Elabscience, China) and Cy3 (red, 1:100; Elabscience, China) were used as secondary antibodies. Images were observed and photographed using a DM-6B fluorescence microscope (Leica, Germany) or an Axio Observer fluorescence microscope (Zeiss, Germany). For cell counting, fields with 300–500 cells were chosen at random. ImageJ was used to calculate the percentage of positive cells in vitro and the percentage of positive regions in vivo.

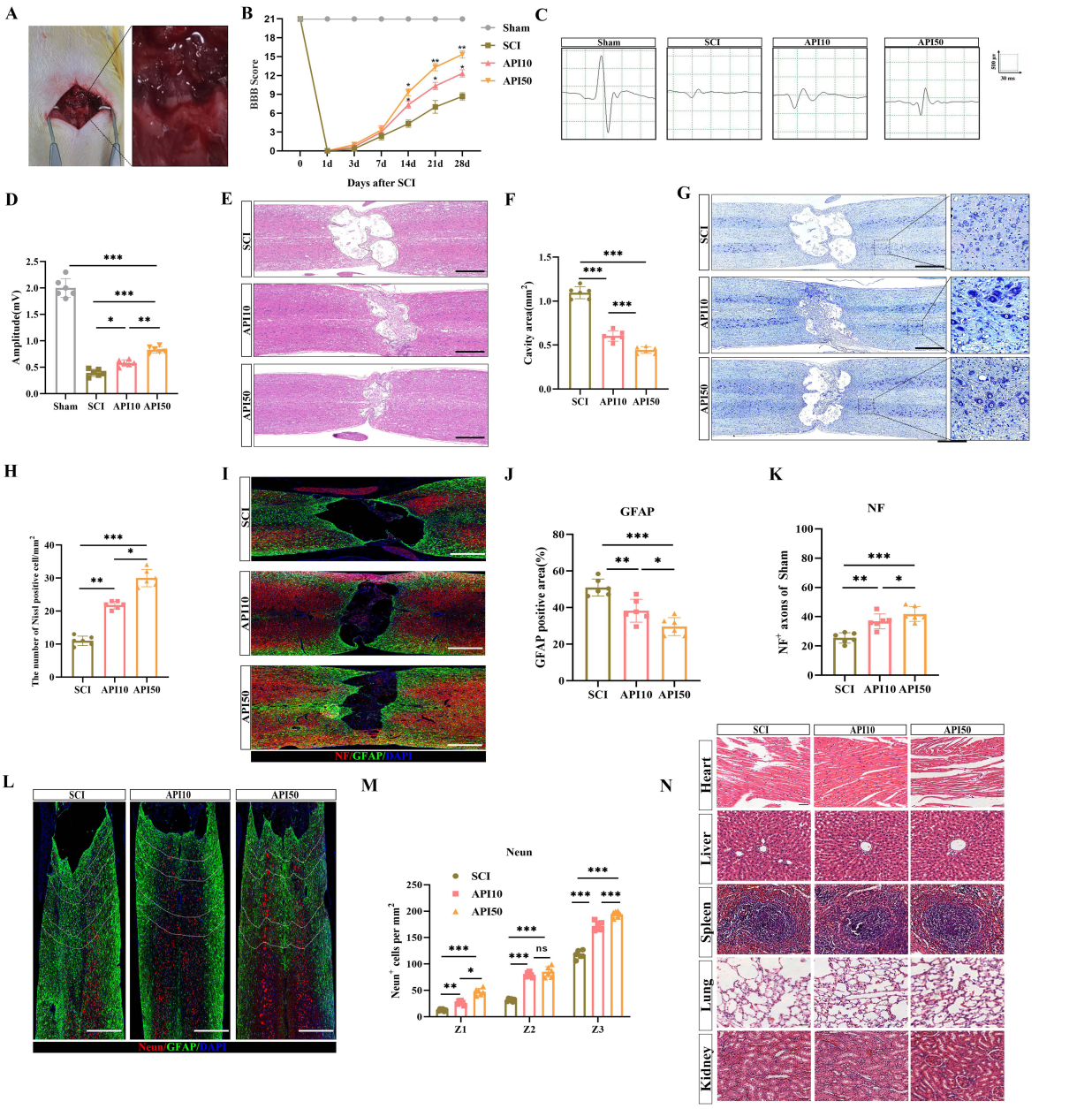


**Figure 1** API promoted motor function recovery and neural regeneration after SCI. (**A**) A representative macroscopic image of spinal cord injury model construction. (**B**) BBB scores for hindlimb motor function in rats across different time points (eg, 1, 7, 14, 21, and 28 days post-injury). The BBB score is a well-established metric for assessing hindlimb locomotor function in rodents, with higher scores indicating better functional recovery. Results demonstrated that rats in the API treatment group exhibited significantly improved motor function over time compared to control groups (n = 12 per group). (**C** and **D**) Motor evoked potential (MEP) recordings. (**C**) Representative MEP waveforms; (**D**) quantitative analysis of MEP amplitudes. MEP amplitudes reflect the integrity of neural signal transmission from the brain to the muscles, with higher amplitudes indicating better neural conduction. The API treatment group showed a significant increase in MEP amplitude, suggesting partial restoration of neural conduction function (n = 6 per group). (**E** and **F**) Histological evaluation of spinal cord tissue using H&E staining. (**E**) Representative H&E-stained cross-sectional images; (**F**) quantitative analysis of cavity area. H&E staining enables visualization of overall tissue architecture and injury-induced cavitation. A smaller cavity area indicates less severe tissue damage. The API treatment group exhibited a significantly reduced cavity area, indicating a protective effect against structural damage (scale bar: 500 μm; n = 6 per group). (**G** and **H**) Nissl staining of spinal cord sections. (**G**) Representative Nissl-stained images; (**H**) quantification of Nissl body density (per mm²). Nissl bodies are cytoplasmic markers of neuronal integrity and protein synthesis activity. A higher number of Nissl bodies reflects greater neuronal survival and functional preservation. The API treatment group showed significantly more Nissl-positive neurons compared to the injury control group, indicating enhanced neuronal survival (scale bar: 500 μm; n = 6 per group). (**I–K**) Immunofluorescence staining for nerve fibers (NF, red) and astrocytic marker GFAP (green). (**I**) Representative merged fluorescence images; (**J**) quantification of GFAP-positive area intensity, reflecting the extent of glial scar formation; (**K**) relative density of NF-positive axons normalized to the sham group, used to assess axonal preservation and regeneration. The API treatment group exhibited increased NF+ axon density and reduced GFAP expression, suggesting that API promotes axonal regeneration and mitigates glial scar formation (scale bar: 500 μm; n = 6 per group). (**L** and **M**) Immunofluorescence staining for neuronal nuclei (NEUN, red) and GFAP (green). (**L**) Representative images; (**M**) quantification of NEUN+ cell density (per mm²) in the Z1–Z3 regions adjacent to the injury core. NEUN+ cells represent viable neurons. The API treatment group showed a significant increase in NEUN+ cell density, indicating that API enhances neuronal survival in the perilesional area (scale bar: 500 μm; n = 6 per group). (**N**) HE staining depicting histopathological features of heart, liver, spleen, lung, and kidney in different rat groups 28 days post-injury (scale bar = 50μm,n = 6 per group) *P<0.05, **P < 0.01,***P<0.001, ns P>0.05.


https://doi.org/10.2147/JIR.S549251

## Hematoxylin-Eosin (HE) Staining

Rats were perfused transcardially with 0.9% saline, followed by fixation in 4% PFA. A 1 cm segment of the injured spinal cord was excised, post-fixed overnight in 4% PFA, embedded in paraffin, and sectioned. Sections were stained with HE according to the manufacturer's instructions: immersed in hematoxylin for 5 min, rinsed with double-distilled water, and counterstained with eosin for 1 min. Images were obtained via light microscopy for subsequent analysis.

## Nissl Staining

Nissl staining was performed in accordance with the manufacturer's protocol. Briefly, sections were incubated in Nissl stain at 37°C for 10 min, rinsed with double-distilled water for 5 s, and dehydrated in 95% ethanol for 5 s. Images were obtained using light microscopy for subsequent analysis.

## Cell Culture and Treatment

The BV2 microglial cell line was obtained from Pricella Biotechnology Co., Ltd. (CL-0493, Wuhan, China). Cells were maintained in Dulbecco's Modified Eagle Medium (PM150210, Pricella) supplemented with 10% TransSerum® FQ foetal bovine serum (FS30102, TransGen Biotech, Beijing, China) and 1% penicillin-streptomycin (FG101-01, TransGen Biotech). A microglial pyroptosis model mimicking spinal cord injury was established by stimulating cells with lipopolysaccharide (LPS, 100 ng/mL) for 24 h, followed by ATP (5 mM) for 1 h. API was dissolved in 0.1% DMSO and used to pre-treat cells at a concentration of 100 μM for 24 h. Cells were subsequently treated with the mitophagy inhibitor Mdivi-1 (10 μM, MCE, HY-15886, USA) or the autophagy agonist Urolithin A (5 μM, MCE, HY-100599, USA) for 24 h. Cells were divided into five groups: control, LPS/ATP group, LPS/ATP + API, LPS/ATP + UA, and LPS/ATP + API + Mdivi-1.

## Cell Counting Kit-8 Assay

BV2 cells ($5 \times 10^3$ cells/100 μL/well) were seeded into 96-well plates and incubated for 24 h. After treatment, 10 μL of Cell Counting Kit-8 (CCK-8) reagent (C0037, Beyotime Biotechnology) was added, and cells were incubated for a further 2 h. Optical density (OD) at 450 nm was measured using a microplate reader (LUX, Thermo, USA) to assess cell viability.

## Enzyme-Linked Immunosorbent Assay (ELISA)

Spinal tissue was homogenised on ice, centrifuged at 5,000 × g for 5–10 min, and the supernatant was collected. BV2 cells ($1 \times 10^5$ cells/well) were treated as described, and culture supernatants were harvested. Levels of TNF-α and IL-1β in tissue and cell supernatants were quantified using ELISA kits in accordance with the manufacturer's instructions.

## ROS Assay

BV2 cells ($1 \times 10^5$ cells/well) were seeded and treated as described. Intracellular ROS levels were measured using the dihydroethidium (DHE) fluorescent probe (Beyotime, S0033S, Shanghai, China). Cells were washed twice with cold PBS, incubated with diluted 2',7'-Dichlorodihydrofluorescein diacetate at 37°C for 20 min, and then washed three times with serum-free medium. ROS fluorescence was visualised under a fluorescence microscope (DM6B, Leica, Wetzlar, Germany). For tissue ROS detection, warm sections were stained with the DHE working solution at 37°C for 30 min, washed three times with PBS, and counterstained with DAPI. Sections were imaged under the same microscope.

## Quantitative RT-PCR

Total RNA was extracted from tissues, cells, and exosomes using TRIzol reagent (Gibco). Briefly, 1 mL of TRIzol was added, and the mixture was transferred to a 1.5 mL EP tube. Following the addition of 200 μL chloroform, the sample was centrifuged at 12,000 × g for 15 minutes at 4 °C. The supernatant was carefully aspirated, and an equal volume of isopropanol was added. The mixture was then centrifuged again under the same conditions (12,000 × g for 15 minutes at 4 °C). After removing the supernatant, 75% ethanol was added, and the sample was centrifuged twice for 5 minutes each at 12,000 × g and 4 °C. Finally,

**Table 1** Primer Sequences

| Genes | Forward 5′-3′ | Reverse 5′-3′ |
|---|---|---|
| *Nlrp3* | GTGGAGATCCTAGGTTTCTCTG | CAGGATCTCATTCTCTTGGATC |
| *Asc* | GGAGGGGTATGGCTTGGAG | TGAGTGCTTGCCTGTGTTGGT |
| *Gapdh* | GACATGCCGCCTGGAGAAAC | AGCCCAGGATGCCCTTTAGT |

the RNA pellet was resuspended in double distilled water ($ddH_2O$), and the RNA concentration was quantified. Subsequently, cDNA was synthesized from 1 μg of RNA template using the Superscript III RT Reaction Mix (Invitrogen). RT–PCR was performed in a 10 μL reaction mixture containing 1.5 μL of cDNA, 2.5 μL of $ddH_2O$, 1 μL of primer (diluted from 10 μM to 0.4 μM), and 5 μL of SYBR Green, under the following thermal cycling conditions: initial denaturation at 95 °C for 2 min, followed by 40 cycles of denaturation at 95 °C for 30s, annealing at 60 °C for 30s on a 7900 Fast Real-Time PCR System (Applied Biosystems). Gene expression was normalised to glyceraldehyde 3-phosphate dehydrogenase (GAPDH) and analysed using the $2^{-}\Delta\Delta CT$ method. Primer sequences are listed in the Table 1.

## Propidium Iodide (PI) Staining

An apoptosis and necrosis detection kit (C1056, Beyotime Biotechnology, China) incorporating PI staining was used to assess cell death. BV2 cells were cultured in six-well plates and treated as previously described. After treatment, cells were washed twice with cold PBS and then stained with Hoechst 33342 (5 μg/mL) and PI (2 μg/mL) at 4°C for 30 min. A final wash with cold PBS was performed before visualisation under a fluorescence microscope (DM6B, Leica, Wetzlar, Germany).

## Statistical Analysis

Statistical analyses were conducted using SPSS software version 16.0 (Chicago, IL, USA) and GraphPad Prism version 8. Data are presented as means ± standard deviations. Statistical significance was assessed using Student's two-sample t-test or one-way analysis of variance with Tukey's post hoc test.Non-parametric data were analysed using the Mann–Whitney *U*-test or the Kruskal–Wallis test. A $p < 0.05$ was considered statistically significant.

# Results

## API Improves Motor Function Recovery and Neural Regeneration After SCI

To investigate whether API promotes motor function recovery and neural regeneration following SCI, we systematically evaluated the effects of varying concentrations of API in rats with SCI. The BBB scores showed that rats treated with 10 mg/kg and 50 mg/kg of API exhibited significantly higher scores compared to untreated controls starting from day 14 post-injury, with a more pronounced therapeutic effect observed at the higher concentration (Figure 1B). Neuroelectrophysiological assessments corroborated these findings, revealing substantial restoration of neural electrical signals in the API-treated groups relative to controls (Figure 1C and D). Histological analyses were then conducted to further characterise the effects of API on neural recovery. HE staining revealed significant scar cavity formation at the injury site, which was notably reduced following API administration (Figure 1E and F). Nissl staining showed that API markedly attenuated neuronal death in the peri-lesional region compared to controls (Figure 1G and H). Immunofluorescence staining further demonstrated that API not only reduced the GFAP-positive glial scar area but also facilitated the growth of NF-positive axons (Figure 1I–K) and promoted neuronal survival (Figure 1L and M). Subsequently, we evaluated the safety profile of Coordinated PBM in rats. Histological analysis of visceral morphology, including H&E staining of the heart, liver, spleen, lungs, and kidneys, revealed that the organ structures remained intact and showed no significant differences compared to those in the SCI group (Figure 1N). These findings suggest that API promotes nerve regeneration and functional recovery following spinal cord injury in rats without inducing apparent systemic toxicity.

## API Suppresses NLRP3 Inflammasome Activation and Pyroptosis in Microglia After SCI

To evaluate changes in microglial pyroptosis following SCI, we quantified the expression of pyroptosis-associated proteins in microglia. Tissue fluorescence analysis showed that the expression levels of NLRP3 and GSDMD in IBA1-positive microglia were significantly elevated post-SCI, peaking at day 3 (Figure 2A–D). This suggests that SCI triggers activation of the NLRP3 inflammasome in microglia, leading to pyroptosis. To examine the impact of API on neuroinflammation and pyroptosis, we measured inflammatory markers and pyroptosis-associated proteins following API treatment for 3 days. ELISA results demonstrated that API significantly suppressed the expression of pro-inflammatory cytokines TNF-α and IL-1β (Figure 2E and F). Given that NLRP3 inflammasome formation involves key components NLRP3 and ASC, we assessed their mRNA levels via PCR. API treatment significantly downregulated *Nlrp3* and *Asc* mRNA expression in spinal cord tissue compared to untreated controls (Figure 2G and H). Fluorescence staining confirmed that API substantially reduced NLRP3 and GSDMD protein expression in microglia at the lesion site (Figure 2A–D).Together, these findings suggest that API alleviates neuroinflammation and inhibits microglial pyroptosis after SCI.

## API Enhances Mitophagy and Inhibits ROS Production After SCI

To evaluate the effect of API on oxidative stress following SCI, we assessed oxidative stress markers in spinal cord tissue after API treatment (Figure 3A–C). Levels of superoxide dismutase (SOD), glutathione (GSH), and malondialdehyde were significantly elevated in SCI tissues compared to uninjured controls. API treatment reduced these levels markedly, indicating that the inflammatory microenvironment post-SCI exacerbates oxidative stress, which API counteracts by suppressing inflammation-induced ROS production. ROS staining confirmed that both low and high concentrations of API significantly inhibited ROS generation in SCI tissues (Figure 3D and E). Notably, mitochondrial dysfunction is a key source of excess ROS, perpetuating further mitochondrial damage. To determine whether mitophagy contributes to API's protective effects, we examined mitophagy-associated proteins. LC3B expression increased and P62 decreased following API treatment, suggesting enhanced mitophagy and reduced mitochondrial dysfunction (Figure 3F–I).

## API Inhibits NLRP3 Inflammasome Activation and Pyroptosis via Regulating Mitophagy

To determine whether API's anti-pyroptotic effect in microglia involves mitophagy modulation. We treated cells with Mdivi-1. This intervention significantly attenuated the inhibitory effects of API on ROS production and its enhancement of mitophagy in injured spinal cord tissue (Figure 4A–F), suggesting that Mdivi-1 effectively suppresses mitophagy following SCI. Subsequently, ELISA revealed that Mdivi-1 supplementation significantly increased the expression of inflammatory cytokines TNF-α and IL-1β in spinal cord tissue treated with API (Figure 5A and B). Furthermore, compared to the non-supplemented group, Mdivi-1 treatment markedly upregulated the mRNA levels of *Nlrp3* and *Asc* after API administration (Figure 5C and D). Tissue fluorescence staining confirmed that mitophagy inhibition amplified the expression of pyroptosis-related markers NLRP3 and GSDMD in API-treated samples (Figure 5E–H). Collectively, these results demonstrate that API mitigates NLRP3 inflammasome activation and pyroptosis in microglia by regulating mitophagy.

## API Inhibits NLRP3 Inflammasome Activation and Pyroptosis in BV2 Cells

To further elucidate the molecular mechanisms underlying API's inhibitions of microglial pyroptosis, we established a pyroptosis model in BV2 cells using LPS and ATP (LPS/ATP). CCK-8 assay indicated that API at 100 μM exerted no cytotoxic effects on microglia (Figure 6A), supporting its suitability for downstream experiments. ELISA analysis showed that LPS/ATP significantly increased TNF-α and IL-1β production in BV2 cells, whereas API treatment markedly suppressed the release of these cytokines (Figure 6B and C). PCR analysis further revealed that the API significantly downregulated the mRNA expression of *Nlrp3* and *Asc* compared to the LPS/ATP only treatment (Figure 6D and E), indicating effective suppression of the NLRP3 inflammasome activation. Immunofluorescence

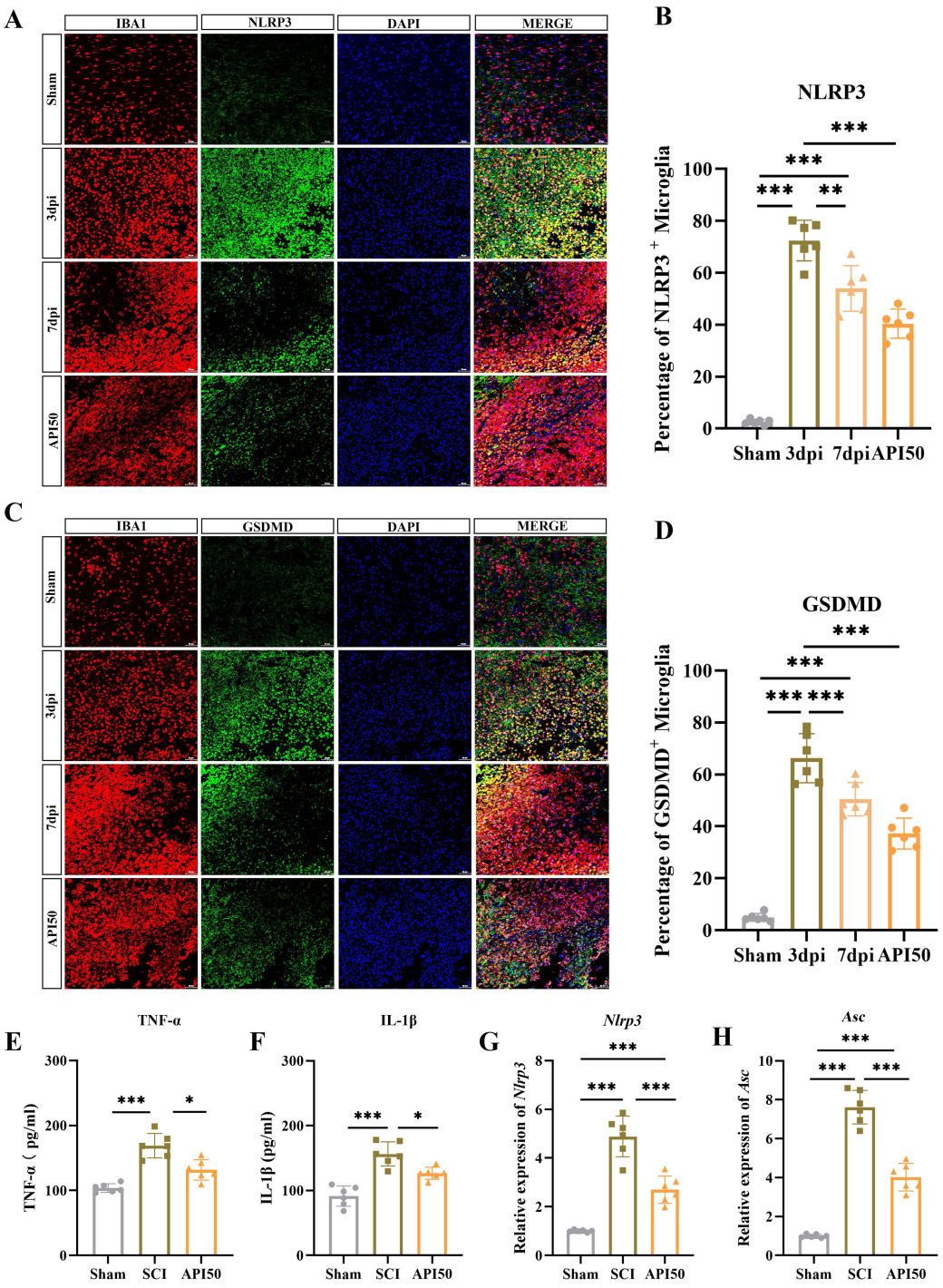


**Figure 2** API inhibited microglial inflammatory response and pyroptosis after SCI. (**A** and **B**) Activation status of the NLRP3 inflammasome in microglia. (**A**) Representative immunofluorescence images showing IBA1 (microglial marker, red) and NLRP3 (green) in spinal cord tissue; (**B**) Quantitative analysis of the percentage of NLRP3-positive microglia. NLRP3 is a critical component of the inflammatory response, and its activation contributes to the progression of neuroinflammation. API treatment significantly reduced the proportion of NLRP3-positive cells, indicating its ability to suppress excessive microglial activation (scale bar: 50 μm; n = 6 per group). (**C** and **D**) GSDMD-mediated pyroptosis in microglia. (**C**) Representative co-localization images of IBA1 (red) and GSDMD (green), a key executor of pyroptosis; (**D**) Quantification of GSDMD-positive microglia. Pyroptosis is an inflammatory form of programmed cell death that exacerbates secondary tissue damage following spinal cord injury. The API treatment group exhibited a marked decrease in GSDMD-positive cells, suggesting that API exerts a protective effect by inhibiting pyroptosis (scale bar: 50 μm; n = 6 per group).(**E** and **F**) Levels of inflammatory cytokines in spinal cord tissue. (**E** and **F**) ELISA was used to measure the concentrations of two key pro-inflammatory cytokines, TNF-α and IL-1β, in spinal cord tissue. These cytokines are central mediators of neuroinflammation, and their levels directly correlate with the severity of the inflammatory response. API treatment led to a significant reduction in both cytokine levels, demonstrating its efficacy in attenuating post-injury neuroinflammatory processes (n = 6 per group).(**G** and **H**) Expression of inflammasome-related genes. (**G** and **H**) Relative mRNA expression levels of Nlrp3 and Asc—two core components of the NLRP3 inflammasome—were assessed by quantitative PCR. Higher gene expression levels indicate greater activation of the inflammatory signaling pathway. API treatment significantly downregulated the expression of both genes, providing molecular evidence that API inhibits inflammasome activation and downstream inflammatory signaling (n = 6 per group).*P<0.05, **P<0.01,***P<0.001.


https://doi.org/10.2147/JIR.S549251

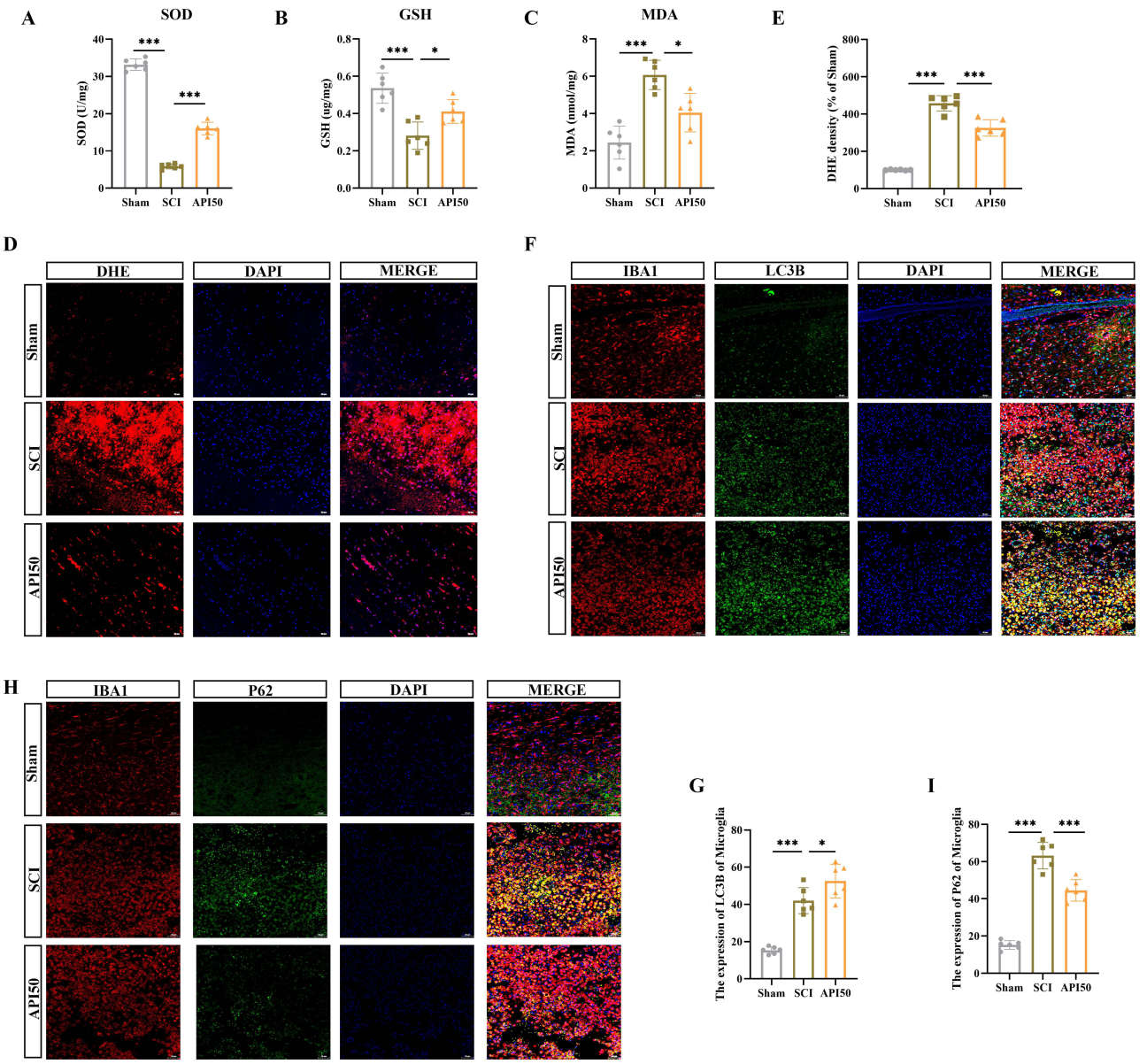


**Figure 3** API enhanced microglial mitophagy and inhibited ROS after SCI. (**A–C**) Assessment of oxidative stress levels in the spinal cord injury region. (**A–C**) present quantitative analyses of superoxide dismutase (SOD) activity, glutathione (GSH) levels, and malondialdehyde (MDA) content in spinal cord tissues across experimental groups. SOD and GSH are key antioxidant enzymes; higher enzymatic activity correlates with enhanced scavenging of reactive oxygen species. MDA is a well-established biomarker of lipid peroxidation, with elevated levels reflecting increased oxidative damage. API treatment significantly elevated SOD and GSH activities while reducing MDA levels, demonstrating its protective effect against oxidative stress following spinal cord injury (n = 6 per group). (**D** and **E**) Measurement of reactive oxygen species (ROS) levels in spinal cord tissue. (**D**) Representative DHE-stained images showing ROS distribution (increased red fluorescence indicates higher ROS levels); (**E**) quantitative analysis of DHE fluorescence intensity normalized to the sham group. ROS are highly reactive molecules that contribute to oxidative damage when accumulated excessively. API treatment significantly reduced ROS levels, indicating its capacity to restore redox homeostasis in the injured spinal cord (scale bar: 50 μm; n = 6 per group). (**F** and **G**) Expression of the autophagy marker LC3B in microglia. (**F**) Representative immunofluorescence images of IBA1 (microglial marker, red) and LC3B (autophagosome marker, green); (**G**) quantification of LC3B-positive microglia. LC3B upregulation is indicative of enhanced autophagic activity, a crucial cellular mechanism for removing damaged organelles and proteins. API treatment increased the proportion of LC3B-positive microglia, suggesting that it enhances autophagy and may contribute to cellular stability following injury (scale bar: 50 μm; n = 6 per group). (**H** and **I**) Expression of the autophagic flux-related protein P62 in microglia. (**H**) Representative co-localization images of IBA1 (red) and P62 (green), a substrate protein that accumulates when autophagic flux is impaired. (**I**) Quantitative analysis of P62-positive microglia. Accumulation of P62 typically reflects defective autophagy. The API treatment group showed a significant decrease in P62-positive cells. Combined with the observed increase in LC3B, these findings support the conclusion that API enhances autophagic flux in microglia, facilitating the clearance of damaged proteins and potentially mitigating neuroinflammation (scale bar: 50 μm; n = 6 per group).*P<0.05, ***P<0.001.

staining corroborated these findings, demonstrating that API reduced GSDMD and NLRP3 protein expression in microglia following LPS/ATP treatment (Figure 6F–I). In addition, PI staining confirmed reduced cell death in the API group compared to the LPS/ATP group (Figure 6J and K).

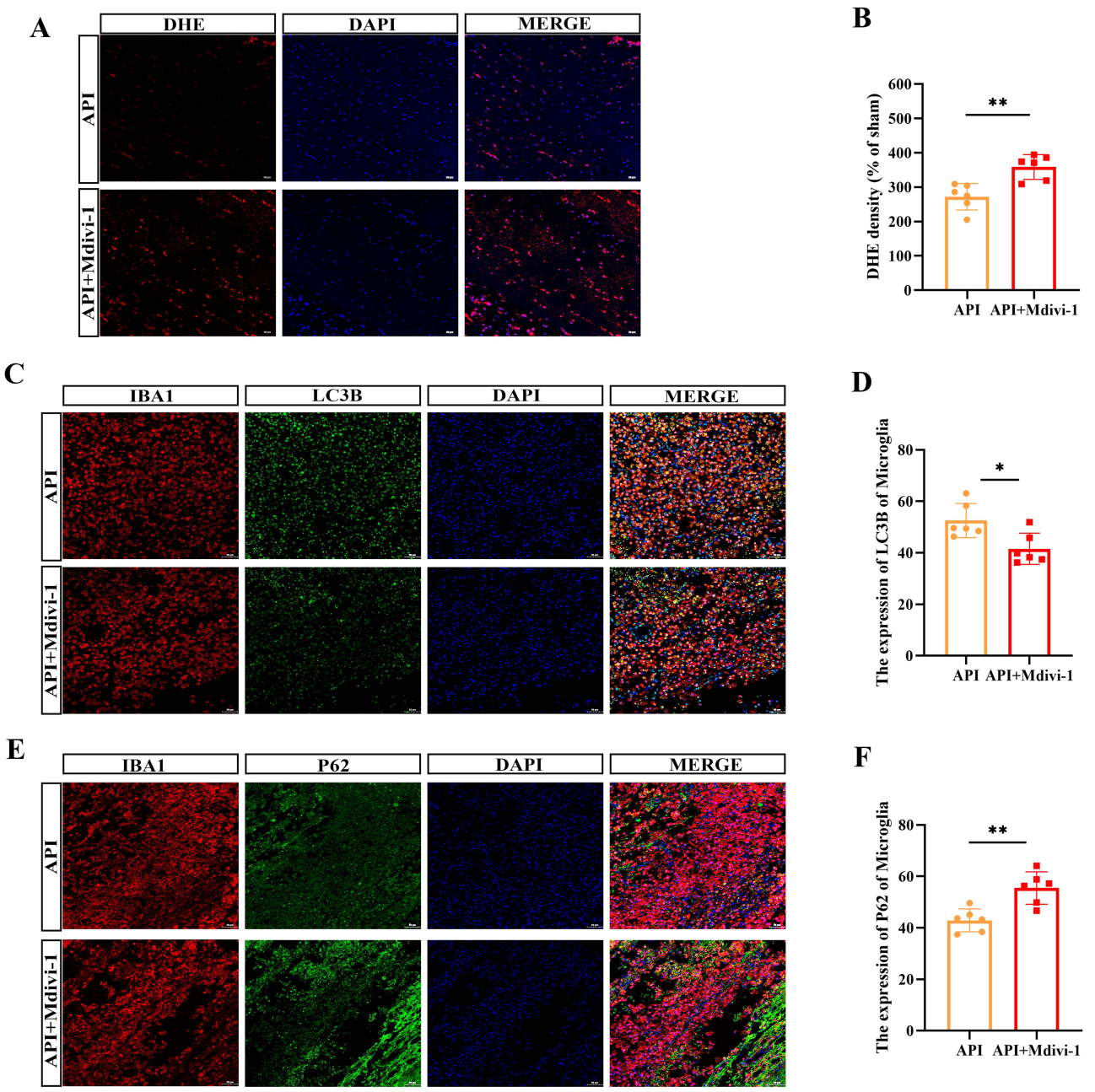


**Figure 4** Mdivi-1 inhibited the regulation of microglial mitophagy by API after SCI. (**A** and **B**) Detection of reactive oxygen species (ROS) in spinal cord tissues.(**A**) Representative images of spinal cord sections stained with the DHE fluorescent probe, where red fluorescence intensity reflects ROS levels; (**B**) Quantitative analysis of DHE fluorescence intensity normalized to the sham group. Excessive ROS contributes to cellular damage, and API treatment significantly reduced ROS levels, demonstrating its antioxidant protective effect (scale bar: 50 μm; n = 6 per group). (**C** and **D**) Expression of LC3B, a marker of autophagic activity in microglia. (**C**) Representative immunofluorescence images of IBA1 (microglial marker, red) and LC3B (autophagosome marker, green); (**D**) Quantification of LC3B-positive microglia. Increased LC3B puncta indicate enhanced autophagic activity. API treatment significantly increased the proportion of LC3B-positive cells, suggesting that it promotes microglial autophagy and facilitates the clearance of damaged cellular components (scale bar: 50 μm; n = 6 per group). (**E** and **F**) Expression of P62, a marker of impaired autophagic flux.(**E**) Representative co-localization images of IBA1 (red) and P62 (green, autophagic substrate); (**F**) Quantitative analysis of P62-positive microglia. Accumulation of P62 indicates impaired autophagic flux. API treatment significantly reduced P62 levels, suggesting that it enhances autophagic flux and supports cellular homeostasis (scale bar: 50 μm; n = 6 per group). *P<0.05, **P<0.01.

## API Promotes Mitophagy to Inhibit NLRP3 Inflammasome Activation and Pyroptosis in BV2 Cells

To validate the anti-pyroptotic effects of API via mitophagy modulation, BV2 cells were co-treated with Mdivi-1 and the autophagy agonist ursolic acid (UA), both known for their neuroprotective properties. Fluorescence analysis revealed that


https://doi.org/10.2147/JIR.S549251

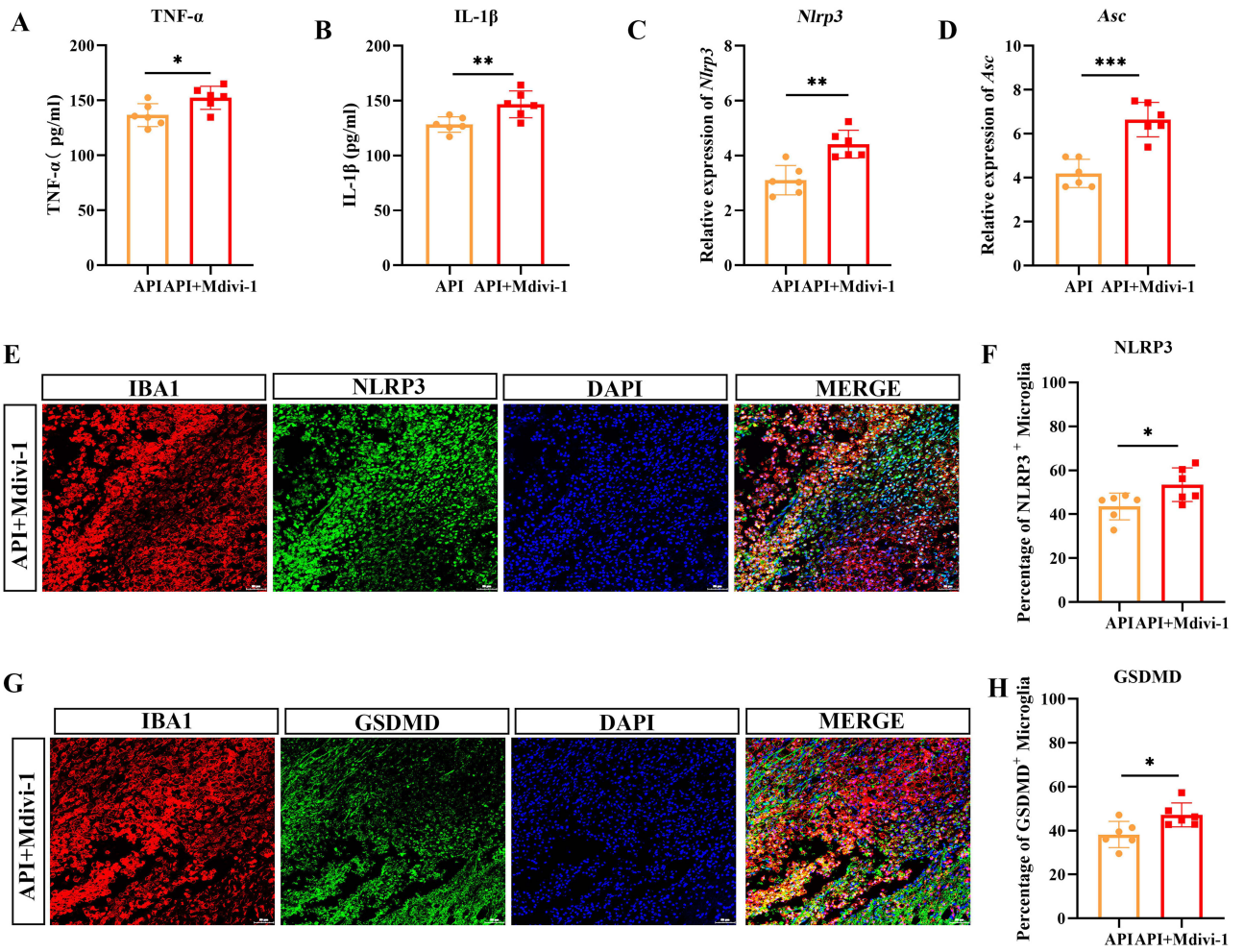


**Figure 5** API inhibited pyroptosis and inflammatory response of microglia by promoting mitophagy after SCI. (**A** and **B**) Levels of pro-inflammatory cytokines in spinal cord tissue.(**A** and **B**) ELISA measurements of TNF-α and IL-1β concentrations. These cytokines are central mediators of neuroinflammation, and their elevation exacerbates tissue damage. API treatment significantly decreased both cytokine levels, indicating its potent anti-inflammatory effect (n = 6 per group). (**C** and **D**) Expression of inflammasome-related genes. (**C** and **D**) qPCR analysis of Nlrp3 and Asc mRNA expression. Higher expression levels reflect greater inflammasome activation. API treatment markedly downregulated both genes, providing molecular evidence of its anti-inflammatory mechanism (n = 6 per group). (**E** and **F**) Activation of the NLRP3 inflammasome in microglia. (**E**) Representative immunofluorescence images of IBA1 (red) and NLRP3 (green); (**F**) Quantification of NLRP3-positive microglia. NLRP3 is a key sensor in inflammasome activation. API treatment reduced NLRP3-positive cell counts, indicating suppression of inflammasome activation (scale bar: 50 μm; n = 6 per group). (**G** and **H**) Microglial pyroptosis status.(**G**) Representative images of IBA1 (red) and GSDMD (green, pyroptosis executor); (**H**) Quantification of GSDMD-positive microglia. Pyroptosis is a pro-inflammatory form of programmed cell death that amplifies neural injury. API treatment significantly reduced GSDMD-positive cells, demonstrating its protective effect against pyroptosis (scale bar: 50 μm; n = 6 per group). *P<0.05, **P<0.01,***P<0.001.

LPS/ATP significantly increased the expression of mitophagy-related proteins P62 and LC3B. API treatment enhanced the LC3B expression and reduced the P62 accumulation, similar to UA. However, these regulatory effects were markedly suppressed when Mdivi-1 was co-administered (Figure 7A–D). Additionally, LPS/ATP significantly elevated intracellular ROS, which was attenuated by both API and UA; this attenuation was abolished by Mdivi-1 (Figure 7E and F). Immunofluorescence analysis further demonstrated that both API and UA decreased GSDMD and NLRP3 expression in LPS/ATP-treated cells, and this effect was mitigated by Mdivi-1 (Figure 7G–J). Consistently, PI staining revealed that Mdivi-1 aggravated cell death compared with API treatment alone (Figure 7K and L). These results collectively suggest that API promotes mitophagy to alleviate mitochondrial dysfunction and suppress oxidative stress-induced pyroptosis in microglia.

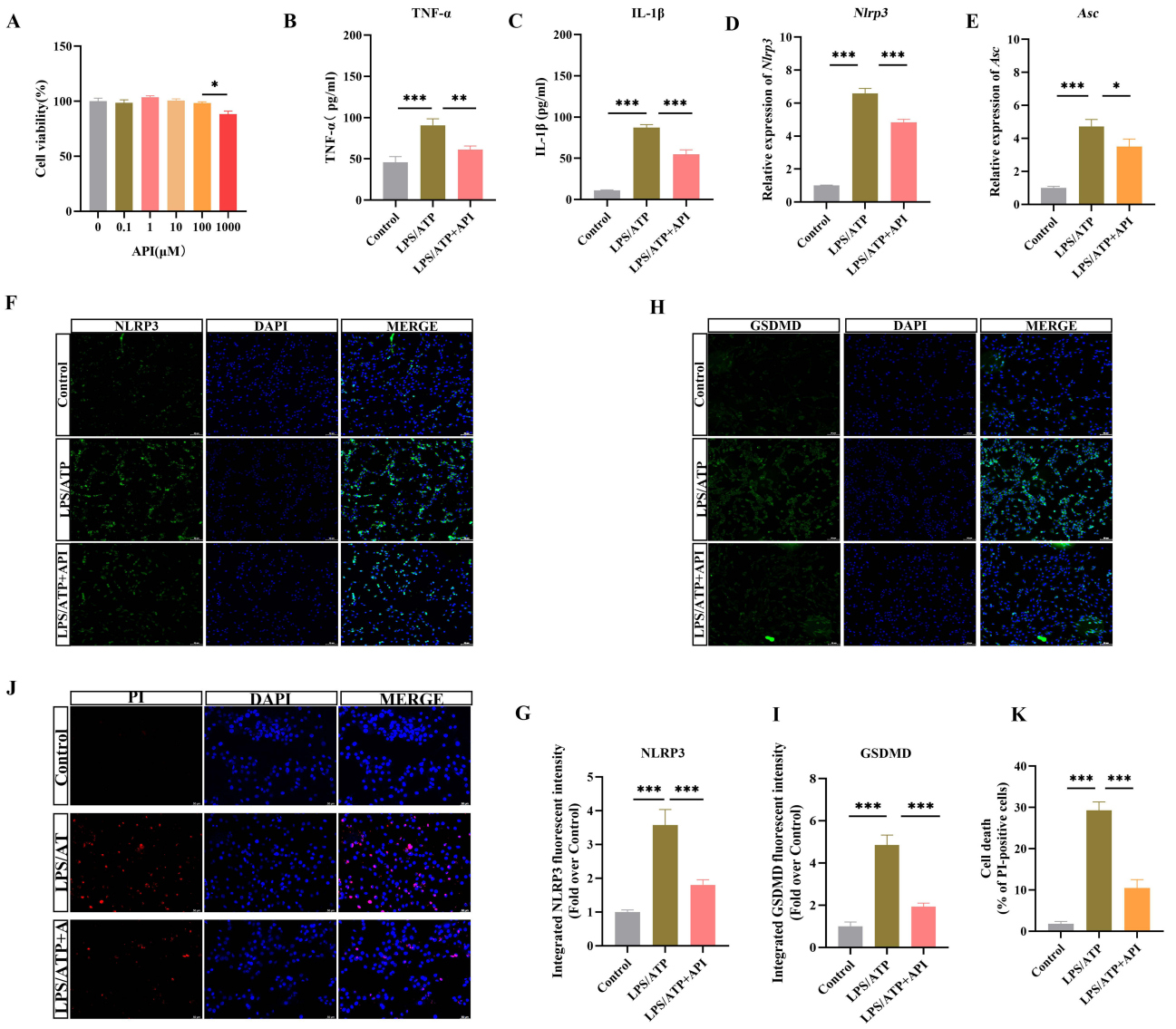


**Figure 6** API inhibited the activation of NLRP3 inflammasome and pyroptosis in BV2 cells. (**A**) Effects of API on cell viability. CCK-8 assay was used to assess the cytotoxicity of API at various concentrations in BV2 cells to identify a non-toxic dose for subsequent experiments (n = 3). (**B** and **C**) Levels of inflammatory cytokines in cell supernatants. (**B** and **C**) ELISA quantification of TNF-α and IL-1β released by BV2 cells. API treatment significantly reduced both cytokine levels, confirming its anti-inflammatory effects in vitro (n = 3). (**D** and **E**) Expression of inflammasome-related genes. (**D** and **E**) qPCR analysis of Nlrp3 and Asc mRNA expression. API treatment significantly suppressed both genes, demonstrating its ability to inhibit inflammasome signaling at the transcriptional level (n = 3). (**F** and **G**) expression of NLRP3 protein. (**F**) Representative immunofluorescence images of NLRP3 (green); (**G**) Quantitative analysis of relative fluorescence intensity (normalized to control). API treatment reduced NLRP3 expression, indicating direct inhibition of inflammasome assembly (scale bar: 50 μm; n = 3). (**H** and **I**) Expression of GSDMD protein. (**H**) Representative images of GSDMD (green); (**I**) Quantitative analysis of fluorescence intensity. GSDMD is a key executor of pyroptosis. API treatment reduced GSDMD levels, indicating suppression of pyroptotic signaling (scale bar: 50 μm; n = 3). (**J** and **K**) Assessment of cell membrane integrity and pyroptosis. (**J**) Representative images of PI (red) staining, which labels cells with compromised membranes; (**K**) Quantification of PI-positive cells. API treatment significantly reduced PI-positive cell counts, directly demonstrating its protective effect against pyroptosis (scale bar: 50 μm; n = 3).*P<0.05, **P<0.01,***P<0.001.

## Discussion

In this study, we demonstrated that API, a natural flavonoid compound, effectively inhibits pyroptosis mediated by neuroinflammation following SCI. API attenuated SCI-induced activation of the NLRP3 inflammasome and suppressed microglial pyroptosis by enhancing mitophagy, thereby promoting neurological functional recovery. Mitophagy acted as a critical mediator of the neuroprotective effects of API. By enhancing mitophagy, API improved mitochondrial quality control, reduced ROS accumulation, and inhibited the release of inflammatory cytokines. Collectively, our findings confirm that API exerts neuroprotective effects after SCI by mitigating neuroinflammation, with its mechanism closely associated with the inhibition of NLRP3 inflammasome activation and microglial pyroptosis through the promotion of mitophagy (Figure 8). This


https://doi.org/10.2147/JIR.S549251

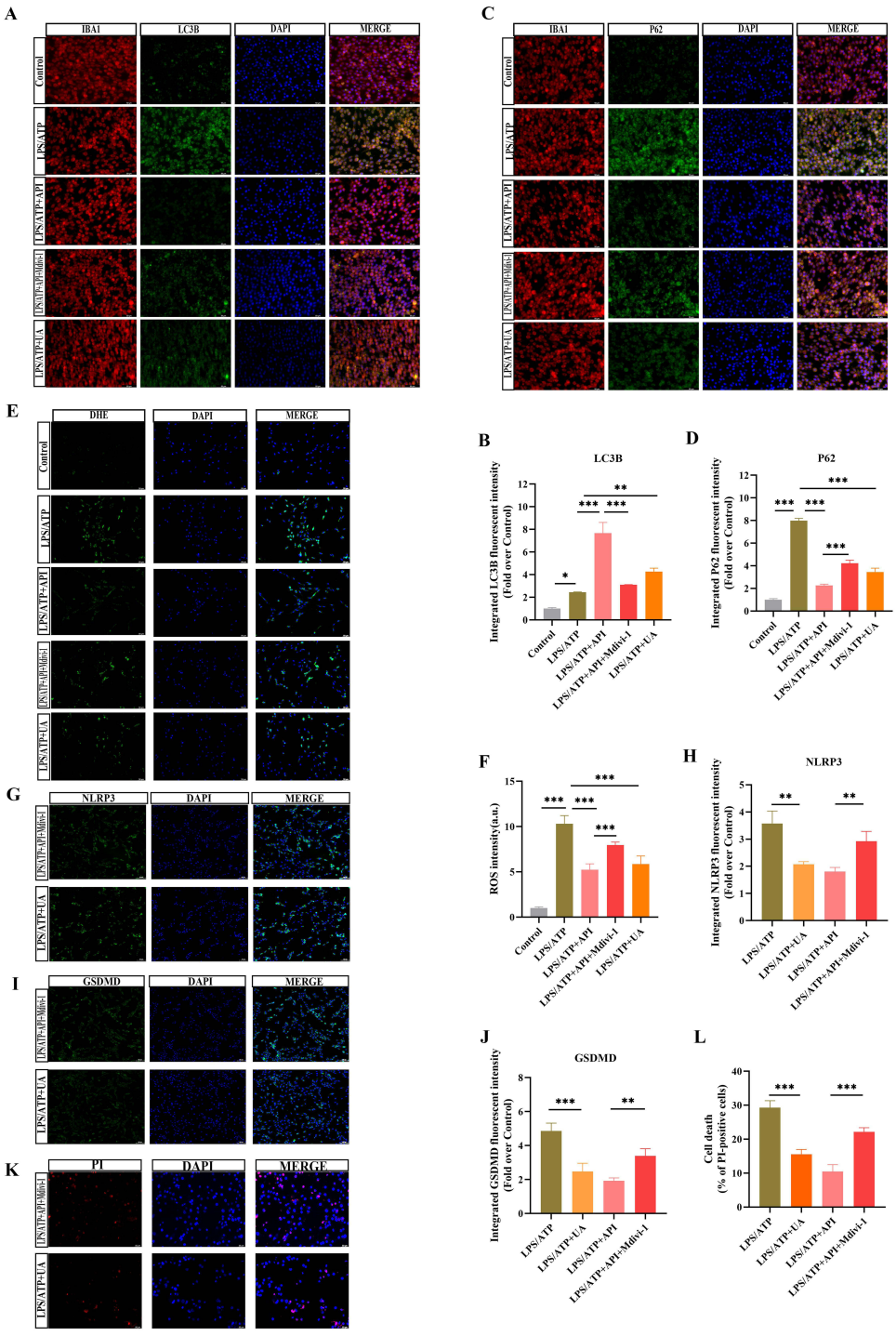


**Figure 7** API inhibited the activation of NLRP3 inflammasome and pyroptosis in BV2 cells by promoting mitophagy. (**A** and **B**) Expression of the autophagy marker LC3B. (**A**) Representative immunofluorescence images of LC3B (green); (**B**) Quantitative analysis of LC3B fluorescence intensity. Increased LC3B puncta indicate enhanced autophagy. API treatment significantly increased LC3B signal, suggesting activation of autophagic processes (scale bar: 50 μm; n = 3). (**C** and **D**) Expression of the autophagic substrate P62. (**C**) Representative images of P62 (green); (**D**) Quantitative analysis of fluorescence intensity. P62 accumulation reflects impaired autophagic flux. API treatment reduced P62 levels, indicating improved autophagic degradation (scale bar: 50 μm; n = 3). (**E** and **F**) Intracellular ROS levels.(**E**) Representative DHE-stained images showing ROS distribution; (**F**) Quantitative analysis of DHE fluorescence intensity (normalized to control). API treatment significantly reduced ROS levels, demonstrating its antioxidant capacity (scale bar: 50 μm; n = 3). (**G** and **H**) Expression of NLRP3 inflammasome proteins. (**G**) Representative images of NLRP3 (green); (**H**) Quantitative analysis of fluorescence intensity. Enhanced autophagy correlated with reduced NLRP3 expression, suggesting that autophagy may facilitate inflammasome clearance (scale bar: 50 μm; n = 3). (**I** and **J**) Expression of GSDMD, the pyroptosis executor protein. (**I**) Representative images of GSDMD (green); (**J**) Quantitative analysis of fluorescence intensity. API treatment reduced GSDMD expression, indicating inhibition of pyroptosis (scale bar: 50 μm; n = 3). (**K** and **L**) Cell death assessment. (**K**) Representative PI (red) staining images; (**L**) Quantification of PI-positive cells. API treatment significantly reduced cell death, providing comprehensive evidence that its protective effects are mediated through autophagy activation, oxidative stress reduction, and inflammation suppression (scale bar: 50 μm; n = 3). *P<0.05, **P<0.01,***P<0.001.

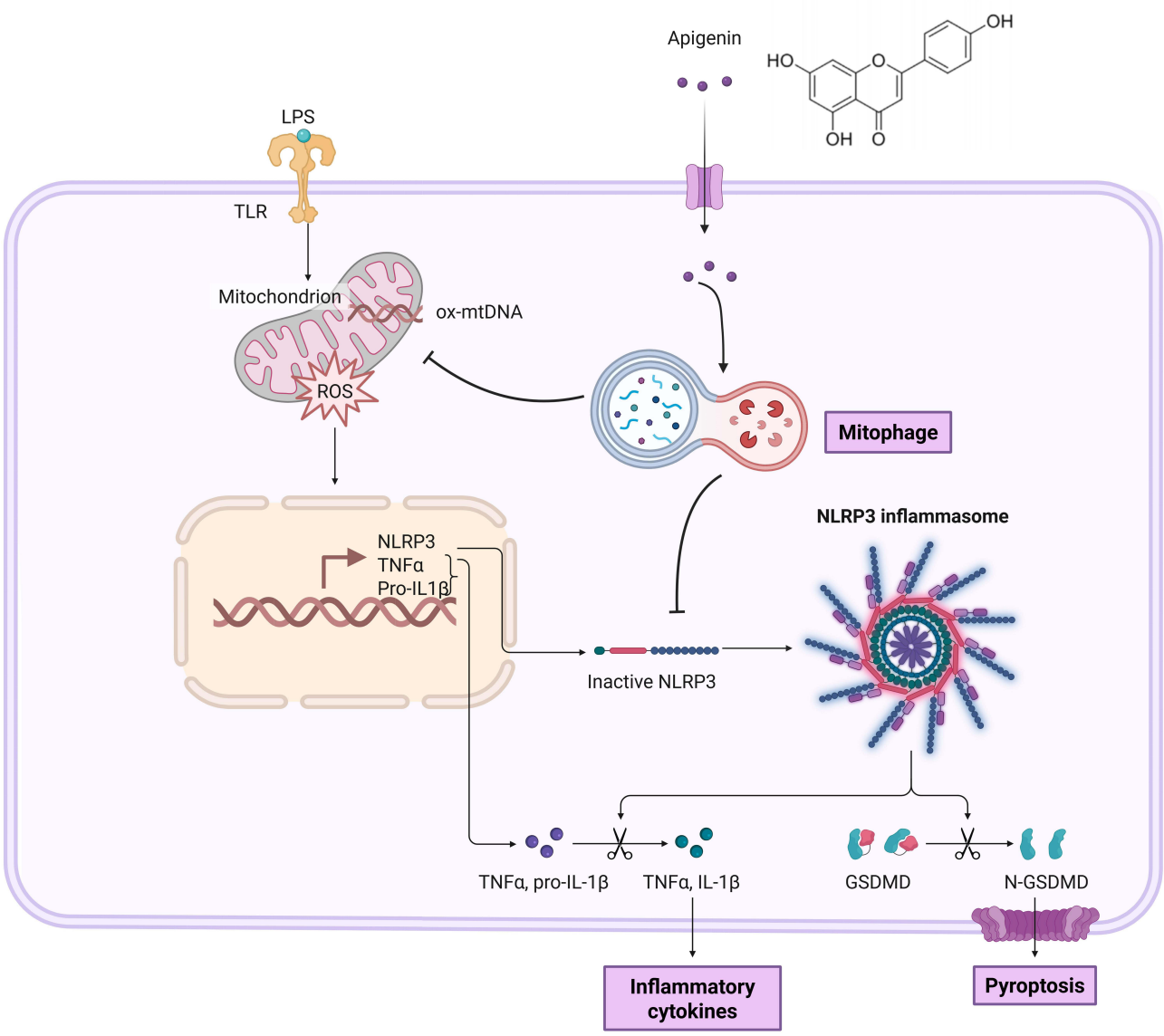


**Figure 8** The schematic diagram illustrates the role and mechanism of API in promoting mitophagy and inhibiting pyroptosis in microglia.

discovery not only elucidates the mechanisms by which natural flavonoids confer neuroprotection but also offers novel insights into the interplay between mitochondrial quality control and inflammatory regulation.

Mitochondria, as central hubs for oxidative stress and inflammatory signalling, play a crucial role in the secondary injury phase of SCI due to their dysfunction.[45–47] Local ischemia and hypoxia in the injured spinal cord lead to MMP collapse, resulting in the release of ROS and mtDNA. Both act as DAMPs that directly activate the NLRP3 inflammasome.[48–50] In this study, API was found to promote mitophagy by increasing the expression of the autophagy marker LC3B and decreasing the level of the autophagy substrate P62. Further intervention experiments using the mitophagy inhibitor Mdivi-1 and the agonist UA confirmed the essential role of mitophagy in API's protective effects: Mdivi-1 reversed the inhibitory effects of API on ROS, NLRP3/GSDMD expression, and inflammatory cytokines, whereas UA mimicked the anti-pyroptotic effects. These findings indicate that API restores mitophagy function, effectively clearing dysfunctional mitochondria and interrupting the vicious cycle of ROS accumulation and NLRP3 activation.

Microglia, as the principal immune effector cells in the spinal cord, contribute to secondary injury following SCI through excessive activation and pyroptosis. On one hand, the release of pro-inflammatory cytokines such as IL-1β and TNF-α during pyroptosis exacerbates blood-spinal cord barrier disruption and neuronal apoptosis.[10–12] On the other hand,


https://doi.org/10.2147/JIR.S549251

pyroptosis-induced membrane perforation and cytoplasmic content release amplify local inflammatory responses.[51–53] Our in vitro and in vivo experiments demonstrated that API significantly reduces pyroptosis markers, including GSDMD-N terminal fragments, and decreases the proportion of TUNEL-positive cells. These results suggest that API exerts a stronger inhibitory effect on microglial pyroptosis than on apoptosis. This effect is closely linked to mitophagy activation, as damaged mitochondria are major sources of ROS and mtDNA, which directly bind to NLRP3 to promote inflammasome assembly.

Notably, there exists a complex interplay between mitophagy and pyroptosis regulation. Under physiological conditions, mitophagy maintains cellular homeostasis by removing dysfunctional mitochondria.[54–56] However, under pathological conditions such as SCI, impaired mitophagy leads to mtDNA and ROS accumulation, which are key pyroptosis triggers.[57,58] In this study, API enhanced mitophagy and accelerated mitochondrial degradation, thereby reducing cytosolic DAMPs. This mechanism is consistent with findings from models of Alzheimer's disease and ischemic stroke, underscoring the conserved role of mitophagy as a gatekeeper of inflammation.

In the field of SCI treatment, API has demonstrated distinct advantages over conventional therapeutic strategies, although it also presents certain limitations. Compared with specific NLRP3 inhibitors, API's multi-target mechanism offers greater clinical relevance. While NLRP3 inhibitors effectively block inflammasome activation, their single-target action may lead to off-target effects that compromise normal immune function. In contrast, API can simultaneously modulate the TGFβ/SMADs signaling pathway to suppress fibrotic scar formation and exert synergistic effects in antioxidation, anti-inflammation, anti-apoptosis, and anti-pyroptosis, thereby more comprehensively addressing the complex pathophysiological processes following SCI. Compared with stem cell therapy, which faces challenges including low delivery efficiency, lack of standardized protocols, and potential immune rejection, API, as a natural flavonoid compound, exhibits notable translational potential. It is widely available, cost-effective to extract, and circumvents the technical complexity and ethical concerns associated with stem cell culture. Preclinical studies have demonstrated that intraperitoneal administration of API dose-dependently enhances motor function recovery in SCI-induced mice, without evident toxic side effects.[41]

Nevertheless, the clinical application of API remains constrained by its pharmacokinetic profile. Research indicates that its oral bioavailability is extremely low, primarily due to gastrointestinal instability and intestinal first-pass metabolism.[36] Although its metabolite, apigenin-7-O-glucuronide, demonstrates improved systemic exposure, this provides a potential avenue for formulation optimization. Moreover, while stem cell therapy may offer long-term neural regeneration potential, current studies on API predominantly focus on its protective effects during the acute injury phase. Its efficacy and long-term safety in treating chronic SCI remain to be fully elucidated. In conclusion, API, as a naturally derived therapeutic agent, holds promising translational potential for SCI treatment; however, its clinical utility requires further enhancement through innovative drug delivery systems (eg, nano-delivery platforms) and combination therapies to address existing limitations.

It is important to acknowledge that this study employed only two API doses (10 and 50 mg/kg) for intervention, without establishing a complete dose-response curve, which introduces certain limitations in the experimental design. The absence of dose-response data prevents precise determination of the minimum effective dose required for neuroprotection, the optimal therapeutic window, and the potential presence of nonlinear effects. Although our animal experiments demonstrated that the 50 mg/kg group exhibited greater improvement in BBB scores compared to the 10 mg/kg group, which suggested a preliminary dose-dependent trend, the lack of intermediate dose groups (eg, 20–30 mg/kg) precluded the possibility of ruling out an effect plateau or identifying a potentially superior dosage. This limitation may compromise the generalizability and translational relevance of the findings to clinical settings. Future studies should incorporate intermediate dose levels (eg, 20–30 mg/kg) to construct a comprehensive dose-response profile and integrate pharmacokinetic parameters (such as plasma exposure) into the analysis. This approach will enable a more accurate definition of the safe and effective dose range for API in SCI treatment. Such refinement will not only clarify its dose-effect relationship but also provide a stronger experimental foundation for further advancements in dosage formulation and combination therapy strategies.

Although this study demonstrated that API at doses of 10 and 50 mg/kg improved motor function in a rat model of SCI, these preclinical findings have not yet translated into clinical benefits. Over the past three decades, more than 50 compounds have shown therapeutic promise in rodent models of SCI, yet fewer than 5% have progressed to Phase III clinical trials. This translational bottleneck primarily stems from substantial interspecies differences between rodents and humans in anatomical structure, pathological response, and pharmacokinetic profiles. Anatomically, the rat spinal cord

has a smaller diameter and a reduced proportion of corticospinal tract fibers compared to humans. Pathologically, post-SCI inflammation in rats typically resolves within two weeks, whereas in humans, inflammatory responses can persist for years, accompanied by more extensive glial scar formation. Pharmacokinetically, the oral bioavailability of API in humans is markedly lower than in rats, and differences in blood-brain barrier permeability hinder effective drug accumulation at the injury site in humans. Furthermore, rodent models often employ standardized injury protocols and early intervention, which do not reflect the clinical heterogeneity and delayed treatment onset observed in human patients. Additionally, current animal models lack clinical relevance, overlook interspecies pharmacokinetic bridging studies, and employ outcome measures that are poorly aligned with patient-centered clinical endpoints, further limiting translational potential. Future research should prioritize the use of clinically relevant chronic SCI models, integrate pharmacokinetic/pharmacodynamic (PK/PD) bridging analyses, and adopt outcome measures that better reflect human clinical needs to bridge the gap between preclinical research and clinical application.

## Conclusion

In summary, our study demonstrates that API alleviates neuroinflammation by inhibiting microglial pyroptosis, thereby facilitating neural regeneration and functional recovery in experimental SCI rats. This protective effect is mediated through the restoration of mitochondrial function via mitophagy activation, reduction of excessive ROS production, and suppression of NLRP3 inflammasome activation and subsequent pyroptosis. These findings support a novel therapeutic strategy for SCI involving API.

## Institutional Review Board Statement

All animal experimental protocols were reviewed and approved by the Anhui Medical University Ethics Committee (LLSC 20242471).All animal experiments comply with the National Standards for Laboratory Animal Welfare issued by the Chinese government (GB/T 35892-2018) and the Guide for the Care and Use of Laboratory Animals (National Research Council, 8th Edition, 2011).All procedures comply with the ARRIVE guidelines.

## Abbreviations

API, Apigenin; SCI, Spinal Cord Injury; NLRP3, NOD-like receptor pyrin domain-containing 3; LPS, lipopolysaccharide; ATP, adenosine triphosphate; ROS, reactive oxygen species; mtDNA, mitochondrial DNA; IL-1β, interleukin-1β; DAMPs, damage-associated molecular patterns; ASC, apoptosis-associated speck-like protein; NF-κB, nuclear factor-κB; GSDMD, gasdermin D; SD, Sprague-Dawley; DMSO, dimethyl sulfoxide; BBB, Basso, Beattie, and Bresnahan; MEPs, motor-evoked potentials; PBS, phosphate-buffered saline; PFA, paraformaldehyde; BSA, bovine serum albumin; DAPI, 4',6-diamidino-2-phenylindole; CCK-8, Cell Counting Kit-8; DHE, dihydroethidium; PI, Propidium Iodide.

## Data Sharing Statement

The data used to support the findings of this study are available from the corresponding author upon request.

## Acknowledgments

We would like to thank the Center for Scientific Research of Anhui Medical University for valuable help in our experiment.

## Author Contributions

Zuomeng Wu and Yunxiao Fang contributed equally to this work and should be considered co-first authors. All authors made a significant contribution to the work reported, whether that is in the conception, study design, execution, acquisition of data, analysis and interpretation, or in all these areas; took part in drafting, revising or critically reviewing the article; gave final approval of the version to be published; have agreed on the journal to which the article has been submitted; and agree to be accountable for all aspects of the work.

## Funding

This work was supported by grants from the National Natural Science Foundation of China (no. 81472088) and the Key Research and Development Project of Anhui Province (no. 2022e07020046).

## Disclosure

The authors declare no conflict of interest.

## References

1. Hu X, Xu W, Ren Y, et al. Spinal cord injury: molecular mechanisms and therapeutic interventions. *Signal Transduct Target Ther*. 2023;8(1):245. doi:10.1038/s41392-023-01477-6
2. Anjum A, Yazid MD, Fauzi Daud M, et al. spinal cord injury: pathophysiology, multimolecular interactions, and underlying recovery mechanisms. *Int J Mol Sci*. 2020;21(20):7533. doi:10.3390/ijms21207533
3. Jiang B, Sun D, Sun H, et al. Prevalence, incidence, and external causes of traumatic spinal cord injury in China: a nationally representative cross-sectional survey. *Front Neurol*. 2021;12:784647. doi:10.3389/fneur.2021.784647
4. Spinal Cord Injury 2016. Facts and figures at a glance. *J Spinal Cord Med*. 2016;39(4):493–494. doi:10.1080/10790268.2016.1210925
5. Xiang YT, Wu JJ, Ma J, et al. Peripheral nerve transfers for dysfunctions in central nervous system injuries: a systematic review. *Int J Surg*. 2024;110(6):3814–3826. doi:10.1097/JS9.0000000000001267
6. Zheng B, Tuszynski MH. Regulation of axonal regeneration after mammalian spinal cord injury. *Nat Rev Mol Cell Biol*. 2023;24(6):396–413. doi:10.1038/s41580-022-00562-y
7. Bradbury EJ, Burnside ER. Moving beyond the glial scar for spinal cord repair. *Nat Commun*. 2019;10(1):3879. doi:10.1038/s41467-019-11707-7
8. Al Mamun A, Wu Y, Monalisa I, et al. Role of pyroptosis in spinal cord injury and its therapeutic implications. *J Adv Res*. 2020;28:97–109. doi:10.1016/j.jare.2020.08.004
9. Wei FL, Wang TF, Wang CL, et al. Cytoplasmic escape of mitochondrial DNA mediated by Mfn2 downregulation promotes microglial activation via cGas-Sting axis in spinal cord injury. *Adv Sci*. 2024;11(4):e2305442. doi:10.1002/advs.202305442
10. Li L, Acioglu C, Heary RF, Elkabes S. Role of astroglial toll-like receptors (TLRs) in central nervous system infections, injury and neurodegenerative diseases. *Brain Behav Immun*. 2021;91:740–755. doi:10.1016/j.bbi.2020.10.007
11. Liu Z, Yao X, Jiang W, et al. Advanced oxidation protein products induce microglia-mediated neuroinflammation via MAPKs-NF-κB signaling pathway and pyroptosis after secondary spinal cord injury. *J Neuroinflammation*. 2020;17(1):90. doi:10.1186/s12974-020-01751-2
12. Zhou X, Wahane S, Friedl MS, et al. Microglia and macrophages promote corralling, wound compaction and recovery after spinal cord injury via Plexin-B2. *Nat Neurosci*. 2020;23(3):337–350. doi:10.1038/s41593-020-0597-7
13. Li J, Yang D, Li Z, et al. PINK1/Parkin-mediated mitophagy in neurodegenerative diseases. *Ageing Res Rev*. 2023;84:101817. doi:10.1016/j.arr.2022.101817
14. Lin Q, Li S, Jiang N, et al. Inhibiting NLRP3 inflammasome attenuates apoptosis in contrast-induced acute kidney injury through the upregulation of HIF1A and BNIP3-mediated mitophagy. *Autophagy*. 2021;17(10):2975–2990. doi:10.1080/15548627.2020.1848971
15. Bi Y, Liu S, Qin X, et al. FUNDC1 interacts with GPx4 to govern hepatic ferroptosis and fibrotic injury through a mitophagy-dependent manner. *J Adv Res*. 2024;55:45–60. doi:10.1016/j.jare.2023.02.012
16. Liu R, Xu C, Zhang W, et al. FUNDC1-mediated mitophagy and HIF1α activation drives pulmonary hypertension during hypoxia. *Cell Death Dis*. 2022;13(7):634. doi:10.1038/s41419-022-05091-2
17. Su L, Zhang J, Gomez H, Kellum JA, Peng Z. Mitochondria ROS and mitophagy in acute kidney injury. *Autophagy*. 2023;19(2):401–414. doi:10.1080/15548627.2022.2084862
18. Han X, Xu T, Fang Q, et al. Quercetin hinders microglial activation to alleviate neurotoxicity via the interplay between NLRP3 inflammasome and mitophagy. *Redox Biol*. 2021;44:102010. doi:10.1016/j.redox.2021.102010
19. Zhang Z, Li M, Li X, et al. Glutamine metabolism modulates microglial NLRP3 inflammasome activity through mitophagy in Alzheimer's disease. *J Neuroinflammation*. 2024;21(1):261. doi:10.1186/s12974-024-03254-w
20. Ayyubova G, Madhu LN. Microglial NLRP3 inflammasomes in Alzheimer's disease pathogenesis: from interaction with autophagy/mitophagy to therapeutics. *Mol Neurobiol*. 2025;62(6):7124–7143. doi:10.1007/s12035-025-04758-z
21. Zhou F, Lian W, Yuan X, et al. Cornuside alleviates cognitive impairments induced by Aβ1-42 through attenuating NLRP3-mediated neurotoxicity by promoting mitophagy. *Alzheimers Res Ther*. 2025;17(1):63. doi:10.1186/s13195-025-01715-9.]
22. López-Doménech G, Howden JH, Covill-Cooke C, et al. Loss of neuronal Miro1 disrupts mitophagy and induces hyperactivation of the integrated stress response. *EMBO J*. 2021;40(14):e100715. doi:10.15252/embj.2018100715
23. Cao Y, Zheng J, Wan H, et al. A mitochondrial SCF-FBXL4 ubiquitin E3 ligase complex degrades BNIP3 and NIX to restrain mitophagy and prevent mitochondrial disease. *EMBO J*. 2023;42(13):e113033. doi:10.15252/embj.2022113033
24. Zhou J, Qiu J, Song Y, et al. Pyroptosis and degenerative diseases of the elderly. *Cell Death Dis*. 2023;14(2):94. doi:10.1038/s41419-023-05634-1
25. Hsu SK, Li CY, Lin IL, et al. Inflammation-related pyroptosis, a novel programmed cell death pathway, and its crosstalk with immune therapy in cancer treatment. *Theranostics*. 2021;11(18):8813–8835. doi:10.7150/thno.62521
26. Liu P, Zhang Z, Chen H, Chen Q. Pyroptosis: mechanisms and links with diabetic cardiomyopathy. *Ageing Res Rev*. 2024;94:102182. doi:10.1016/j.arr.2023.102182
27. Wei Y, Yang L, Pandeya A, Cui J, Zhang Y, Li Z. Pyroptosis-Induced inflammation and tissue damage. *J Mol Biol*. 2022;434(4):167301. doi:10.1016/j.jmb.2021.167301
28. Dubyak GR, Miller BA, Pearlman E. Pyroptosis in neutrophils: multimodal integration of inflammasome and regulated cell death signaling pathways. *Immunol Rev*. 2023;314(1):229–249. doi:10.1111/imr.13186

29. Coll RC, Schroder K, Pelegrín P. NLRP3 and pyroptosis blockers for treating inflammatory diseases. *Trends Pharmacol Sci*. 2022;43(8):653–668. doi:10.1016/j.tips.2022.04.003
30. Luo L, Liu M, Fan Y, et al. Intermittent theta-burst stimulation improves motor function by inhibiting neuronal pyroptosis and regulating microglial polarization via TLR4/NFκB/NLRP3 signaling pathway in cerebral ischemic mice. *J Neuroinflammation*. 2022;19(1):141. doi:10.1186/s12974-022-02501-2
31. Wang F, Liang Q, Ma Y, et al. Silica nanoparticles induce pyroptosis and cardiac hypertrophy via ROS/NLRP3/Caspase-1 pathway. *Free Radic Biol Med*. 2022;182:171–181. doi:10.1016/j.freeradbiomed.2022.02.027
32. Li N, Zhou H, Wu H, et al. STING-IRF3 contributes to lipopolysaccharide-induced cardiac dysfunction, inflammation, apoptosis and pyroptosis by activating NLRP3. *Redox Biol*. 2019;24:101215. doi:10.1016/j.redox.2019.101215
33. Xiao Y, Zhao C, Tai Y, et al. STING mediates hepatocyte pyroptosis in liver fibrosis by epigenetically activating the NLRP3 inflammasome. *Redox Biol*. 2023;62:102691. doi:10.1016/j.redox.2023.102691
34. Gu HY, Liu N. Mechanism of effect and therapeutic potential of NLRP3 inflammasome in spinal cord injury. *Exp Neurol*. 2025;384:115059. doi:10.1016/j.expneurol.2024.115059
35. Liu Z, Tu K, Zou P, et al. Hesperetin ameliorates spinal cord injury by inhibiting NLRP3 inflammasome activation and pyroptosis through enhancing Nrf2 signaling. *Int Immunopharmacol*. 2023;118:110103. doi:10.1016/j.intimp.2023.110103
36. Salehi B, Venditti A, Sharifi-Rad M, et al. The therapeutic potential of apigenin. *Int J Mol Sci*. 2019;20(6):1305. doi:10.3390/ijms20061305
37. Wang F, Yan X, Yue A, et al. Apigenin alleviates doxorubicin-induced myocardial pyroptosis by inhibiting glycogen synthase kinase-3β in vitro and in vivo. *Drug Dev Res*. 2024;85(4):e22196. doi:10.1002/ddr.22196
38. Meng Z, Zhu B, Gao M, et al. Apigenin alleviated PA-induced pyroptosis by activating autophagy in hepatocytes. *Food Funct*. 2022;13 (10):5559–5570. doi:10.1039/d1fo03771d
39. Kong S, Xiao Y, Chen L, et al. Apigenin attenuates cisplatin-induced hair cell damage in the zebrafish lateral line. *Food Chem Toxicol*. 2024;194:115099. doi:10.1016/j.fct.2024.115099
40. Weng X, Luo X, Dai X, et al. Apigenin inhibits macrophage pyroptosis through regulation of oxidative stress and the NF-κB pathway and ameliorates atherosclerosis. *Phytother Res*. 2023;37(11):5300–5314. doi:10.1002/ptr.7962
41. Jin Z, Tian L, Zhang Y, et al. Apigenin inhibits fibrous scar formation after acute spinal cord injury through TGFβ/SMADs signaling pathway. *CNS Neurosci Ther*. 2022;28(11):1883–1894. doi:10.1111/cns.13929
42. Wu Z, Han T, Dong Y, et al. Acid-sensing ion channel-1 contributes to the failure of myelin sheath regeneration following spinal cord injury by transcellular delivery of PGE2. *Cell Mol Biol Lett*. 2024;29(1):149. doi:10.1186/s11658-024-00672-9
43. McDonough A, Monterrubio A, Ariza J, Martínez-Cerdeño V. Calibrated forceps model of spinal cord compression injury. *J Vis Exp*. 2015; (98):52318. doi:10.3791/52318
44. Liu Y, Yao F, Li Z, et al. Dynamic phosphorylation of Fascin-1 orchestrates microglial phagocytosis and neurological recovery after spinal cord injury. *J Neuroinflammation*. 2025;22(1):121. doi:10.1186/s12974-025-03445-z
45. Yao S, Pang M, Wang Y, et al. Mesenchymal stem cell attenuates spinal cord injury by inhibiting mitochondrial quality control-associated neuronal ferroptosis. *Redox Biol*. 2023;67:102871. doi:10.1016/j.redox.2023.102871
46. Han Q, Xie Y, Ordaz JD, et al. Restoring cellular energetics promotes axonal regeneration and functional recovery after spinal cord injury. *Cell Metab*. 2020;31(3):623–641.e8. doi:10.1016/j.cmet.2020.02.002
47. Slater PG, Domínguez-Romero ME, Villarreal M, Eisner V, Larraín J. Mitochondrial function in spinal cord injury and regeneration. *Cell Mol Life Sci*. 2022;79(5):239. doi:10.1007/s00018-022-04261-x
48. Wang X, Zhou G, Xiong J, et al. H4K12 lactylation Activated-Spp1 in reprogrammed microglia improves functional recovery after spinal cord injury. *CNS Neurosci Ther*. 2025;31(2):e70232. doi:10.1111/cns.70232
49. Grace PM, Strand KA, Galer EL, et al. Morphine paradoxically prolongs neuropathic pain in rats by amplifying spinal NLRP3 inflammasome activation. *Proc Natl Acad Sci U S A*. 2016;113(24):E3441–E3450. doi:10.1073/pnas.1602070113
50. Yin TC, Li YC, Sung PH, et al. Adipose-derived mesenchymal stem cells overexpressing prion improve outcomes via the NLRP3 inflammasome/DAMP signalling after spinal cord injury in rat. *J Cell Mol Med*. 2023;27(4):482–495. doi:10.1111/jcmm.17620
51. Jiang Z, Zeng Z, He H, et al. Lycium barbarum glycopeptide alleviates neuroinflammation in spinal cord injury via modulating docosahexaenoic acid to inhibiting MAPKs/NF-kB and pyroptosis pathways. *J Transl Med*. 2023;21(1):770. doi:10.1186/s12967-023-04648-9
52. Wang J, Zhang F, Xu H, et al. TLR4 aggravates microglial pyroptosis by promoting DDX3X-mediated NLRP3 inflammasome activation via JAK2/STAT1 pathway after spinal cord injury. *Clin Transl Med*. 2022;12(6):e894. doi:10.1002/ctm2.894
53. Li F, Sun X, Sun K, Kong F, Jiang X, Kong Q. Lupenone improves motor dysfunction in spinal cord injury mice through inhibiting the inflammasome activation and pyroptosis in microglia via the nuclear factor kappa B pathway. *Neural Regen Res*. 2024;19(8):1802–1811. doi:10.4103/1673-5374.389302
54. Liu L, Li Y, Chen G, Chen Q. Crosstalk between mitochondrial biogenesis and mitophagy to maintain mitochondrial homeostasis. *J Biomed Sci*. 2023;30(1):86. doi:10.1186/s12929-023-00975-7
55. Uoselis L, Nguyen TN, Lazarou M. Mitochondrial degradation: mitophagy and beyond. *Mol Cell*. 2023;83(19):3404–3420. doi:10.1016/j.molcel.2023.08.021
56. Wilhelm LP, Zapata-Muñoz J, Villarejo-Zori B, et al. BNIP3L/NIX regulates both mitophagy and pexophagy. *EMBO J*. 2022;41(24):e111115. doi:10.15252/embj.2022111115
57. Wu C, Chen H, Zhuang R, et al. Betulinic acid inhibits pyroptosis in spinal cord injury by augmenting autophagy via the AMPK-mTOR-TFEB signaling pathway. *Int J Biol Sci*. 2021;17(4):1138–1152. doi:10.7150/ijbs.57825
58. Zhang H, Wu C, Yu DD, Su H, Chen Y, Ni W. Piperine attenuates the inflammation, oxidative stress, and pyroptosis to facilitate recovery from spinal cord injury via autophagy enhancement. *Phytother Res*. 2023;37(2):438–451. doi:10.1002/ptr.7625